

Article

Influence of Substrate on the Tribological Behavior of Inconel 625 GMAW Overlays

Demostenes Ferreira Filho ^{1,*}, Daniel Souza ¹, José Lúcio Gonçalves Júnior ¹, Ruham Pablo Reis ², Washington Martins Da Silva Junior ² and Amanda Figueira Tavares ³

¹ School of Electrical, Mechanical, and Computer Engineering, Federal University of Goiás, Goiânia 74690-900, Brazil; daniel.souza@ufg.br (D.S.); jlucio@ufg.br (J.L.G.J.)

² Faculty of Mechanical Engineering, Federal University of Uberlândia, Uberlândia 38408-100, Brazil; ruhamreis@ufu.br (R.P.R.); washington.martins@ufu.br (W.M.D.S.J.)

³ School of Engineering, Federal University of Rio Grande, Rio Grande 96203-900, Brazil; amand.figueira@gmail.com

* Correspondence: demostenesferreira@ufg.br

Abstract: This study investigates the microstructure and tribological behavior of Inconel 625 overlays applied via GMAW (Gas Metal Arc Welding) with and without a 316LSi stainless-steel intermediate layer on top of A36 steel. The microstructural characterization was conducted via FESEM with EDS. The tribological behavior was evaluated using a tribometer in a reciprocating configuration. The results showed that the wear rate of the Inconel 625 weld overlay with the 316LSi intermediate layer was higher than without it. However, no variations were observed in terms of hardness and the friction coefficient of the Inconel 625 weld overlays. The difference in the behavior of the two coatings was justified due to the microstructure morphology found in each case and chemical composition. When applied without the intermediate layer, Inconel 625 coating's structure was dendritic, whereas it was cellular otherwise. An increase in the amount of Nb was observed in the layer deposited over 316LSi. This rise likely led to an increase in the number of precipitates and/or Laves phase formation. Thus, the results indicated that the difference in thermal conductivity and dilution between the stainless and carbon steels modifies the morphology of the microstructure of the Inconel 625 weld overlay, decreasing wear resistance when deposited on top of the stainless steel.

Keywords: Inconel 625; 316LSi stainless steel; A36 steel; GMAW cladding; tribological behavior



Citation: Ferreira Filho, D.; Souza, D.; Gonçalves Júnior, J.L.; Reis, R.P.; Da Silva Junior, W.M.; Tavares, A.F. Influence of Substrate on the Tribological Behavior of Inconel 625 GMAW Overlays. *Coatings* **2023**, *13*, 1454. <https://doi.org/10.3390/coatings13081454>

Academic Editor: Francisco J. Flores-Ruiz

Received: 15 June 2023

Revised: 28 July 2023

Accepted: 31 July 2023

Published: 18 August 2023



Copyright: © 2023 by the authors. Licensee MDPI, Basel, Switzerland. This article is an open access article distributed under the terms and conditions of the Creative Commons Attribution (CC BY) license (<https://creativecommons.org/licenses/by/4.0/>).

1. Introduction

Nickel-based alloys are commonly used in a variety of industrial sectors due to their elevated mechanical properties and corrosion resistance, and the Inconel alloy family responds to most applications. Among them, coatings produced by cladding based on fusion welding are largely employed as this protection-improving process is a low-cost option that enables the protection of other metals when such alloys are applied. As an example, the performance of Inconel 625 (wire feedstock) cladding produced via laser beam welding (LBW) under electrochemical corrosion was investigated by Abioye et al. [1]. This cladding comprised a dendritic matrix and interdendritic precipitates, which were shown to be rich in Mo and Nb. Such a coating exhibited an average microhardness of around 232 ± 4.5 HV and corrosion performances very close to that of the reference Inconel 625, which degrades with increasing Fe dilution. Previous works have presented details of the microstructure and dilution of this kind of coating on different steels [2–4], investigating the microstructure of Inconel 625 coatings that are deposited on top of Inconel 738 substrates via LBW and Gas Tungsten Arc Welding (GTAW) cladding. Austenite, carbide, and Laves phases were observed inside the coatings in both deposition processes, but the LBW coatings displayed a more refined microstructure due to the higher cooling rate achieved.

Antoszczyszyn et al. [5] assessed the impact of dilution on the microstructure and properties of Inconel 625 deposited using the Plasma Transferred Arc (PTA) process on API 5L carbon steel and AISI 316L stainless-steel substrates. They observed differences in the microstructure and properties of the coatings produced, which were associated with the interaction with each substrate. A larger fraction of carbides accounted for the higher hardness (about 235 HV) of the coating when on top of the API 5L carbon steel, whereas the low thermal conductivity of the AISI 316L stainless steel and its higher Fe content in solid solution contributed to the lower hardness in the respective coating.

In addition to corrosion resistance, tribological properties are also critical for a variety of equipment, such as those applied in seawater and its surroundings. Zhang et al. [6] showed that friction coefficients are strongly affected by the tribo-oxidant layer in Inconel coatings, as they revealed the sliding wear behavior of three different Inconel 625 coatings produced via cladding. By selecting the proper combination of materials and design strategy, multilayer coatings might be adapted to reduce friction and increase the wear resistance of mechanical components in a variety of tribological applications [7] whether they are employed in brand-new or restored parts. The main purpose of industrial maintenance is to repair faults caused by friction and contact fatigue. Normally, recoating using a new layer allows the reuse of the part that did not support degradation. Thus, coatings are often used to improve the mechanical properties of tribological pairs [8].

A study on the effect of impact and slip of particles on samples of Inconel 690 showed that the wear produced is more severe when it occurs due to unidirectional movements. For multidirectional wear, in contrast, the debris located inside the wear marks reduces the wear rate but increases the friction coefficient, which is the main mechanism of wear: in this case, abrasion with delamination [9]. Li et al. [10] showed that in annealed coatings of Inconel 600 alloys, the increase in treatment temperature caused grain growth and a consequent reduction in the hardness of the protective material. Subsequent fretting wear tests showed that the reduction in grain size promoted the formation of a transformed tribological structure that produced smaller delamination plates and, therefore, a reduction in wear volume.

Therefore, it is observed that the use of fusion welding for producing claddings enables the application of the Inconel alloy family as coatings in different applications at a relatively low cost, especially if arc processes are employed. However, as aforementioned, it is known from the literature that dilution in steel might significantly influence the microstructure, mechanical properties, and therefore, the tribological behavior of Inconel coatings produced via arc welding processes. One of the ways to reduce the influence of steel dilution in Inconel weld overlays is to insert an intermediate layer between the steel and Inconel sections. In this context, the use of stainless steel for the intermediate layer is adequate because it is compatible with both carbon steel and Inconel alloys in part due to their high chromium content, and using a stainless-steel interlayer as an alternative to using two layers of Inconel to decrease Inconel dilution might be a cost-effective solution to the recurrent dilution issue. Thus, the present work aims to compare tribological behaviors under the sliding wear of Inconel 625 deposited on top of carbon steel via GMAW cladding with and without a stainless-steel intermediate layer and hence analyze the influence of the substrate on the performance of such weld overlays.

2. Materials and Methods

2.1. Materials

The weld overlays were applied via the GMAW process in a constant voltage mode coupled with an industrial robot. ASTM A36 steel was used as the initial substrate, and ER316LSi (316L stainless steel) and ERCrNiMo-3 (Inconel 625) filler metals were used as intermediate and top cladding materials, respectively. The choice of Inconel 625 was based on its extensive applications in power generation and energy sectors, as well as its remarkable utilization in the marine and aerospace industries. The chemical composition of such materials is listed in Table 1. Plates measuring 10 mm in thickness, 100 mm in width,

and 150 mm in length were used for the initial substrate. The Ar with 25% of He was used as shielding gas at 16 L/min.

Table 1. Chemical composition of the A36 steel substrate [11] and of the ER316LSi [12] and ERCrNiMo-3 [13] filler metals in weight percentage (wt%).

Element	Ni	Cr	Mn	Si	Al	Ti	Fe	C	Mo	Nb
A36	0.02	0.02	0.67	0.09	0.03	-	Bal.	0.23	-	-
ER316LSi	13.00	19.00	2.50	0.70	-	-	Bal.	0.03	3.00	-
ERCrNiMo-3	Bal.	22.46	-	-	0.26	0.26	0.14	0.02	8.84	3.46

2.2. Methods

Figure 1 presents the flowchart of the activities developed in this study, which are detailed in Sections 2.2.1–2.2.4.

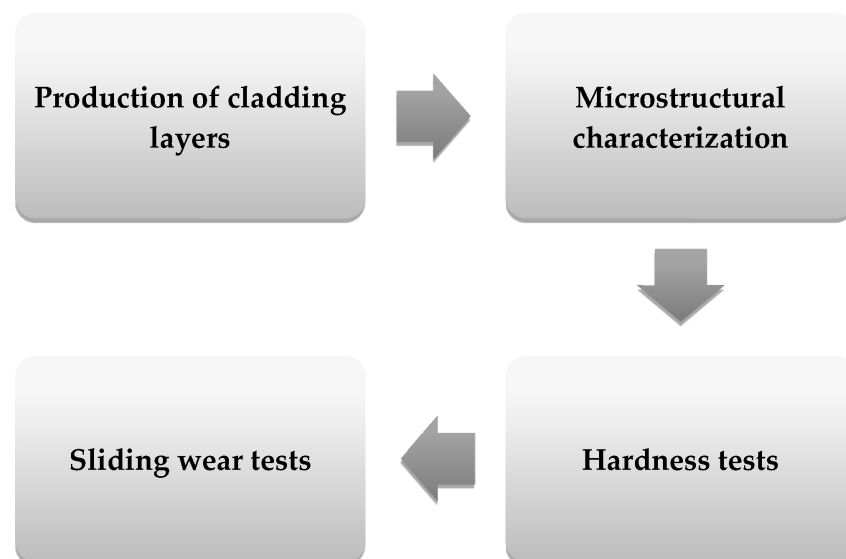


Figure 1. Flowchart of the activities developed in the study with respect to the influence of the substrate on the tribological behavior of the Inconel 625 GMAW overlay.

2.2.1. Production of Cladding Layers

In terms of coatings, two types of samples were produced starting from the ASTM A36 steel substrate:

1. Sample I: GMAW cladding of Inconel 625;
2. Sample M: GMAW cladding of 316LSi stainless steel followed by GMAW cladding of Inconel 625.

Figure 2 schematically shows the sequence of cladding according to the sample type. The waviness observed in the deposition is attributed to the interposition of weld beads, which was performed by overlapping 50% of each previous bead. The parametrization for GMAW claddings is presented in Table 2. The welding current was selected, employing the wire's feed speed at average values of approximately 150 A.

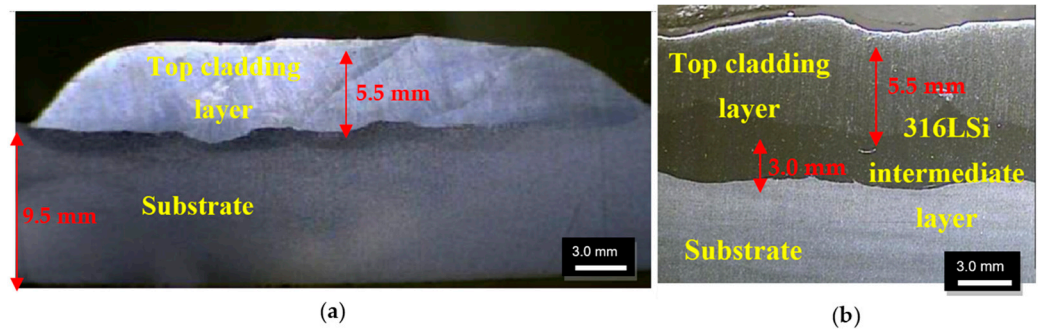


Figure 2. Deposition sequence of cladding layers: (a) Sample I (Inconel 625 weld layer); (b) Sample M (stainless-steel 316LSi intermediate weld layer followed by the top Inconel 625 weld layer).

Table 2. GMAW cladding parametrization of Sample I (Inconel 625 weld layer) and Sample M (stainless-steel 316LSi intermediate weld layer followed by the top Inconel 625 weld layer).

Sample	Layer	Filler Metal	Shielding Gas	Arc Voltage (V)	Wire Feed Speed (m/min)	Welding Travel Speed (cm/min)
I	Top	ERCrNiMo-3	Ar + 25%He	25	12.5	25
M	Intermediate	ER316LSi	Ar + 25%He	25	6.5	25
	Top	ERCrNiMo-3	Ar + 25%He	25	12.5	25

2.2.2. Microstructural Characterization

To obtain insights into the microstructural features of the coatings that were produced, field emission scanning electron microscopy (FESEM) was performed using a MIRA3 TESCAN microscope coupled with an elemental analyzer based on energy dispersive spectroscopy (EDS) and wavelength-dispersive spectroscopy (WDS). To observe the coatings in FESEM equipment, specimens were prepared with typical procedures up to a diamond paste with 0.04 μm as polishing abrasive.

2.2.3. Hardness Tests

Hardness tests were carried out by using Mitutoyo model HV100 equipment with a Vickers indenter at a load of 10 kgf applied for 30 s. Ten hardness measurements were performed directly on the surface of each cladding sample (I and M).

2.2.4. Sliding Wear Tests

Reciprocating wear tests were carried out under dry sliding conditions by using a Plint TE66 tribometer. The counter bodies were AISI 52100 spheres with 10 mm in diameter under a normal load of 20.6 N, resulting in a pressure of 0.17 GPa at 2 Hz. Testing times of 0.5 h were used to assess the wear evolution of the cylinders of the reciprocating wear system and the specimens that were taken from different weld overlays. The variables measured during the tests were friction force and contact potential. For that, an LVDT sensor was incorporated into the tribometer to assess the position of the counterbody against the specimen for each cycle of the reciprocating movement. By using this information, the technique called triboscopy [14–17] was used to produce 3D numerical images where the x-axis represents the position within each cycle, the y-axis represents the number of cycles, and the z-axis represents the measure of friction or contact potential. Three reciprocating tests were performed directly on the surface of each cladding sample (I and M).

3. Results and Discussions

3.1. Microstructural Characterization

Figure 3 presents the SEM images of the top surfaces of the Inconel 625 weld overlay (Sample I) and stainless-steel 316LSi intermediate weld layer followed by the top Inconel

625 weld layer (Sample M). As observed, the cladding layers were formed by columnar dendrites in Sample I and by cellular structure in Sample M.

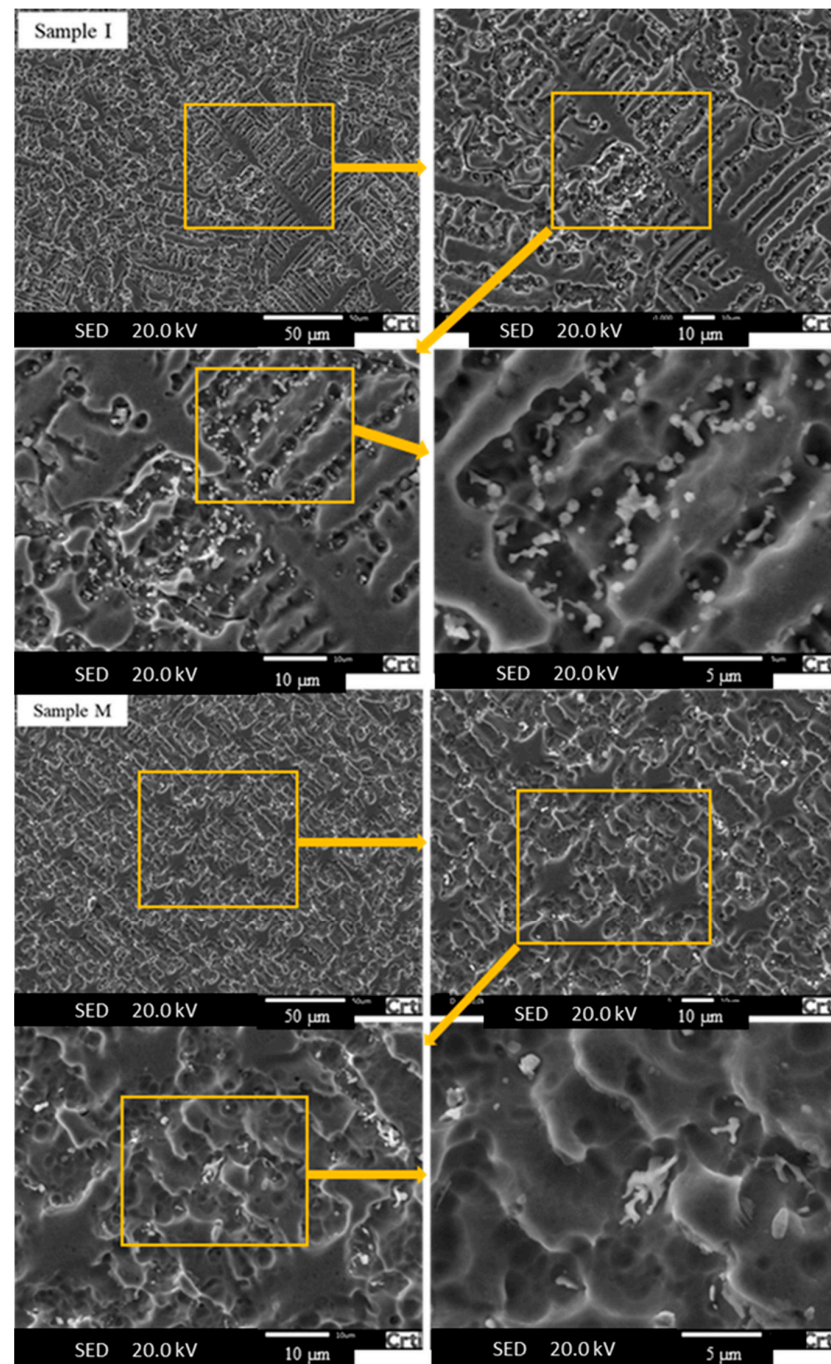


Figure 3. SEM images of the top surfaces of Sample I (Inconel 625 weld layer) and Sample M (stainless-steel 316LSi intermediate weld layer followed by the top Inconel 625 weld layer).

Kim et al. [18] observed equiaxial grain formation in the Inconel 625 overlay produced using electroslag welding, and a cellular structure was observed in the Inconel 625 overlay produced via GMAW by Souza et al. [19]. Lin [20] reports that thermal conductivity may affect grain formation, resulting in modified solidification morphologies. According to Bergman et al. [21], AISI 1010 carbon steel has a thermal conductivity of 63.9 W/m.K against 13.4 W/m.K of the AISI 316 stainless steel. Therefore, the cooling rate of the Inconel layer of Sample M might have been considerably lower than that of Sample I. Thus, the

difference in the thermal conductivity of substrates (carbon steel and 316LSi stainless steel) may explain the difference observed in the morphology of Inconel 625's microstructure in the present study.

Figure 3 also shows a continuous dark dendritic matrix and light contrast precipitates in the interdendritic regions in both samples. An EDS map of Sample I (Figure 4) reveals that the matrix is rich in nickel and chromium and that the interdendritic precipitates are rich in niobium and molybdenum, and the same occurred in Sample M. This occurrence is similar to what has been found in the current literature [1–5,22], but it is important to emphasize that in Sample I, the precipitates are smaller and appear more distributed than those found in Sample M.

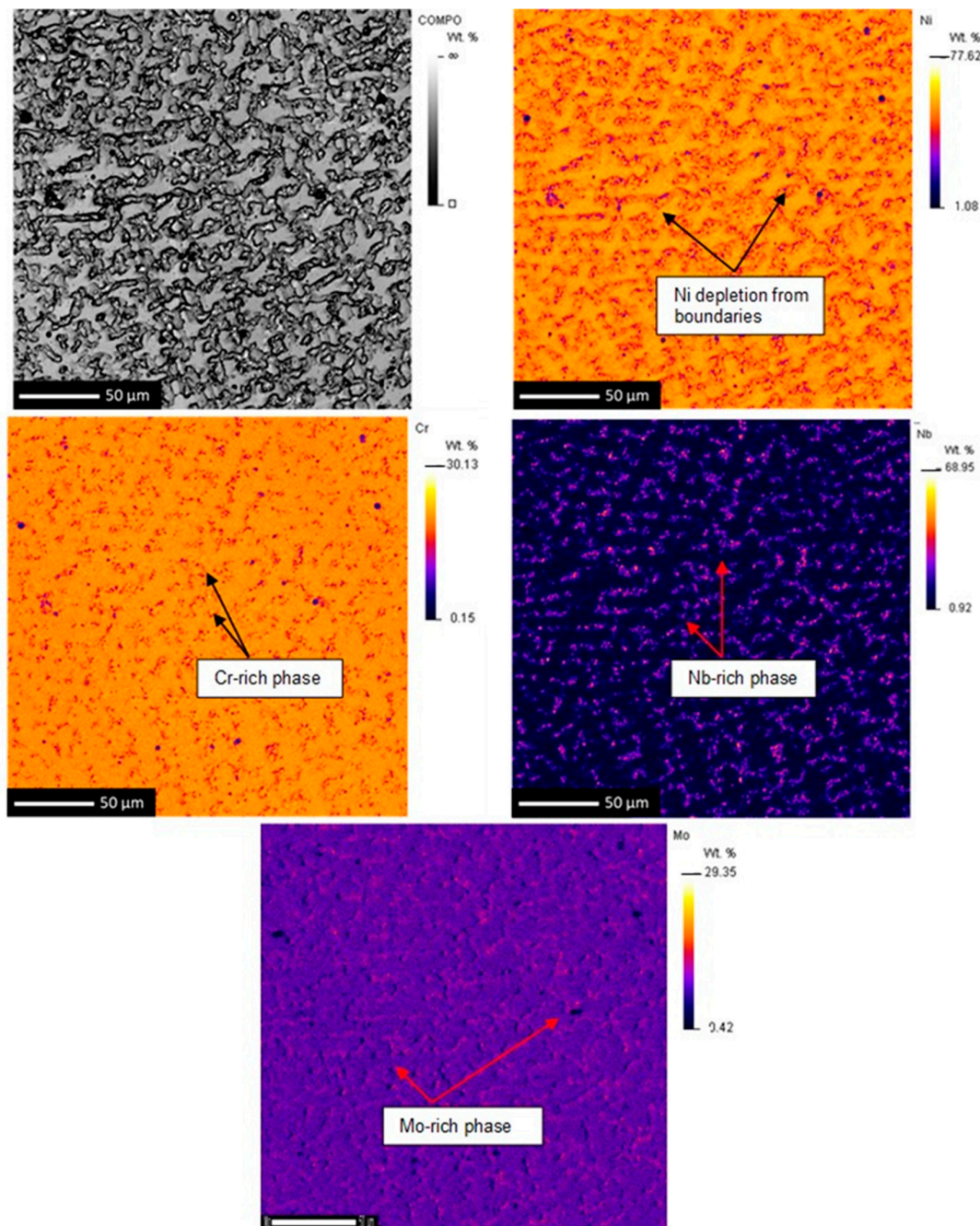


Figure 4. EDS map of Sample I (Inconel 625 weld layer).

An analysis of Figure 4, which illustrates the EDS map of Sample I, confirms the presence of precipitates associated with Nb and Mo elements. Furthermore, an accumulation of Nb and Mo elements is observed in the interdendritic region, which likely contributes to the formation of the Laves phase. This phenomenon was also observed by Sauraw et al. [23] in the case of ERNiCrMo-3 welding, where a significant weight percentage of Nb and Mo was found in interdendritic areas, confirming the precipitation of the Nb-enriched NbC and Laves phases and the Mo-enriched Mo₂C and Laves phases.

The WDS results for both samples are summarized as average terms in Table 3. As observed, the matrix composition in samples I and M is significantly richer in Fe (~24 wt%) when compared with the filler metal, which has Fe contents of only 0.14 wt%. This difference might be attributed to Fe dilution in the substrates (carbon steel plate for Sample I and stainless-steel layer for Sample M), and it is higher than the amount found by Abioye et al. [1]. This scenario is justified by the higher percentage of dilution (approximately 30%) due to the GMAW process and the welding parameters used in the present work. Najafi et al. [24] observed, when depositing three layers of Inconel via GMAW cladding on top of an ASTM A516 Gr 70 plate, that the Fe content in the second and third layers was below 2 wt%. In addition, they also reported that the segregation of Nb and Mo into interdendritic regions contributed to the formation of secondary phases, such as Laves and MC carbide precipitates. At this point, it is essential to emphasize that the distinct dilution mechanisms caused the M sample to exhibit a higher concentration of Nb, potentially contributing to a greater formation of the Laves phase.

Table 3. Chemical composition for Sample I (Inconel 625 weld layer) and Sample M (stainless-steel 316LSi intermediate weld layer followed by the top Inconel 625 weld layer) via WDS (wt%).

Element	Sample I	Sample M
Al	0.27	0.17
Si	0.16	0.24
Ti	1.22	1.22
Cr	18.59	20.54
Mn	0.31	0.54
Ni	41.61	39.25
Nb	4.22	5.03
Mo	8.88	8.74
Fe	24.74	24.27

3.2. Hardness Characterization

The results of the hardness assessment, as shown in Figure 5, indicate that the substrate did not present a significant influence on the Inconel weld overlay. According to Antoszczyszyn et al. [5], the contribution of the substrate to coating properties has three components: it may alter the composition of phases as elements from the substrate are incorporated into the solution solid, it may modify the carbide fraction and distribution, and it may change the thermal cycle undergone by the clad layer.

In this way, the difference in the substrate's thermal conductivity was not a sufficient component to promote hardness modification, despite being capable of affecting the formation and distribution of precipitates, in addition to affecting the morphology of the grains (columnar dendrites for Sample I and cellular structure for Sample M).

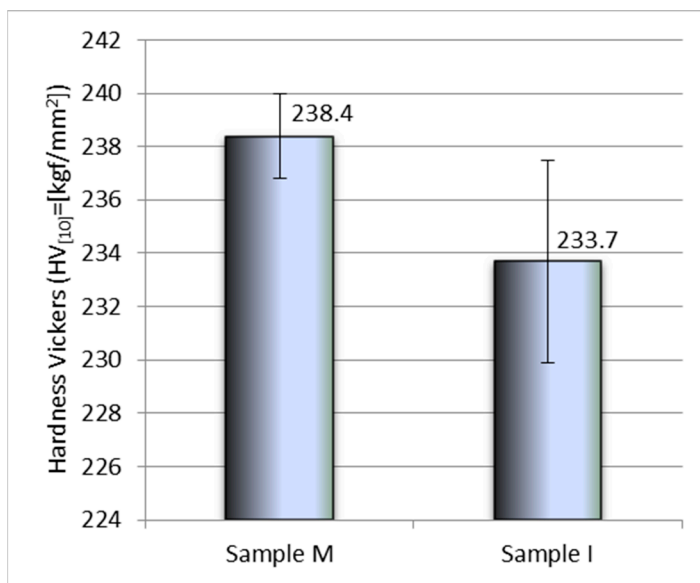


Figure 5. Average hardness levels of Sample I (Inconel 625 weld layer) and Sample M (stainless-steel 316LSi intermediate weld layer followed by the top Inconel 625 weld layer).

3.3. Sliding Wear

As observed in Figure 6, according to the wear assessment, samples I and M did not display differences in the friction coefficient. Corroborating this result, the respective triboscopic maps were constructed at intervals of 7000 cycles during a stability period, and they are shown in Figure 7, where it is possible to observe any variation in the friction coefficient not only in terms of cycles but also along the wear track. Both samples revealed a transient period at the beginning (first cycles) of the tests in the middle of the wear tracks. An increase in the friction coefficient is also observed in both cases at the edges of the wear tracks.

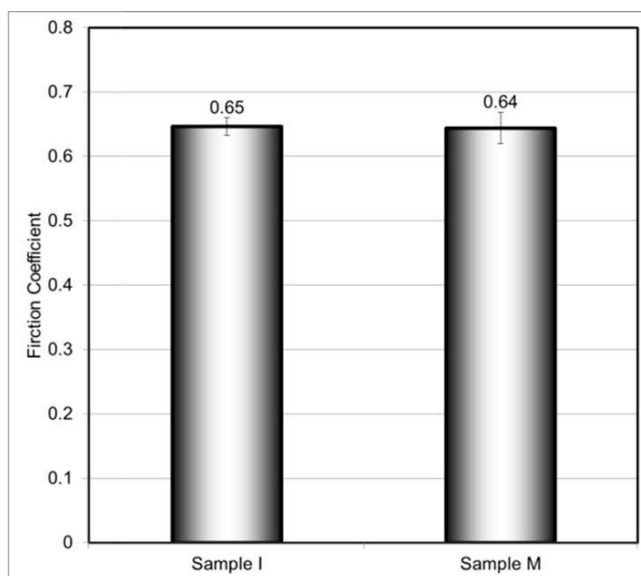


Figure 6. Friction coefficient after the sliding wear test for Sample I (Inconel 625 weld layer) and Sample M (stainless-steel 316LSi intermediate weld layer followed by the top Inconel 625 weld layer).

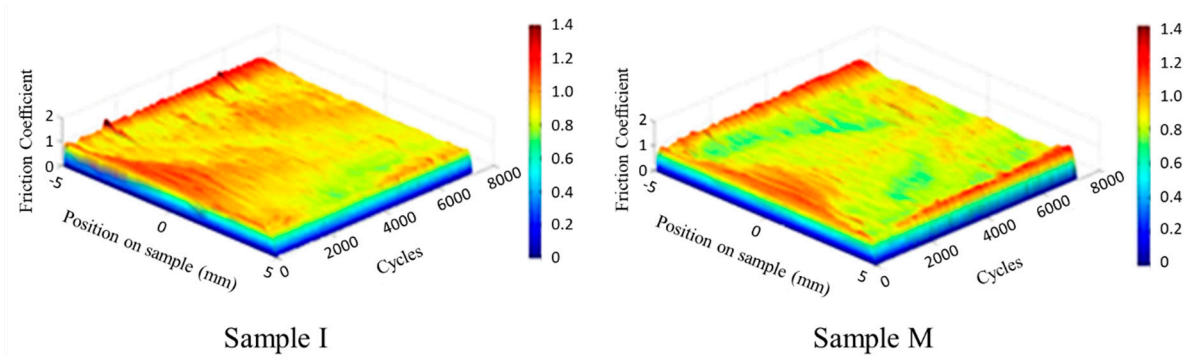


Figure 7. Triboscopic maps for Sample I (Inconel 625 weld layer) and Sample M (stainless-steel 316LSi intermediate weld layer followed by the top Inconel 625 weld layer).

Figure 8 shows the typical wear tracks of samples I and M. Regarding the depth of the wear track, Sample I had an average depth of 128 μm , which was lower than the average depth of 134 μm obtained in Sample M. Additionally, Sample I exhibited a wear volume of 0.718 mm^3 , whereas Sample M had a volume of 0.870 mm^3 . These volumes were obtained from the entire length of the wear tracks. Consequently, it can be concluded that Sample I displayed a wear path with both a smaller volume and depth of wear. The resultant mean values of the specific wear rate are compiled in Figure 9. As observed, Sample I exhibited a lower specific wear rate. But, as aforementioned, samples I and M had similar phase formation and hardness. Thus, the explanation for the higher specific wear rate in Sample M might be related to differences in the microstructure’s morphology if contrasted with Sample I and possibly to an increase in the number of precipitates and/or Laves phase formation.

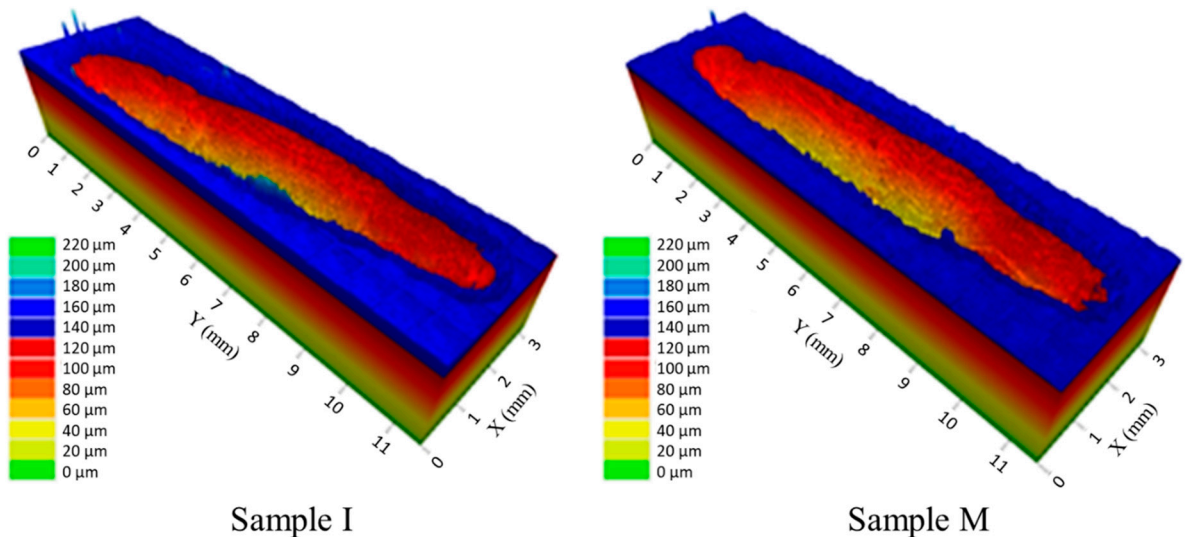


Figure 8. Confocal images of the wear tracks in Sample I (Inconel 625 weld layer) and Sample M (stainless-steel 316LSi intermediate weld layer followed by the top Inconel 625 weld layer).

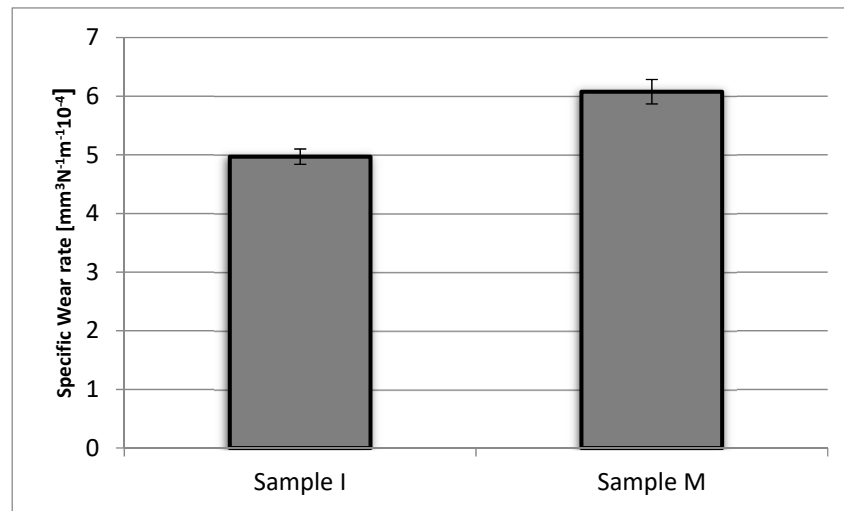


Figure 9. Wear rate after 30 min of sliding for Sample I (Inconel 625 weld layer) and Sample M (stainless-steel 316LSi intermediate weld layer followed by the top Inconel 625 weld layer).

The specific wear rate of the counterbodies was also measured and is shown in Figure 10. It is possible to observe that the counter bodies did not exhibit a significant difference in the specific wear rate compared to the analyzed samples.

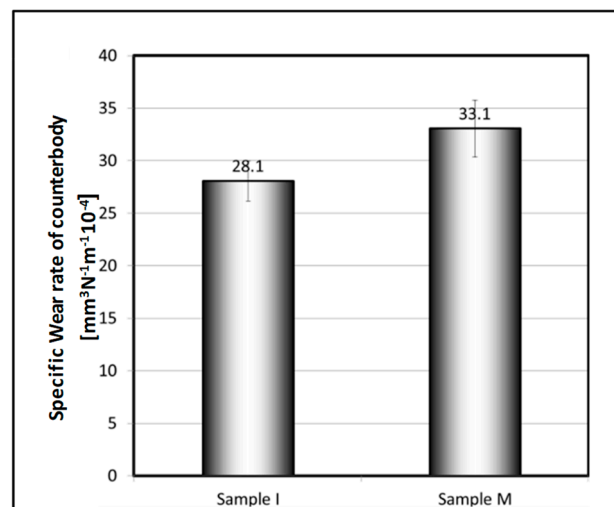


Figure 10. The specific wear rate of counter bodies of sliding for Sample I (Inconel 625 weld layer) and Sample M (stainless-steel 316LSi intermediate weld layer followed by the top Inconel 625 weld layer).

Secondary (Figure 11a,c) and back-scattered (Figure 11b,d) electron images of samples I and M are shown in Figure 11. It is possible to observe similar widths in both cases. It is also possible to observe that the samples revealed different predominant wear mechanisms (abrasive wear in Sample I and adhesive wear in Sample M), which might also play a role in the wear rates that were measured.

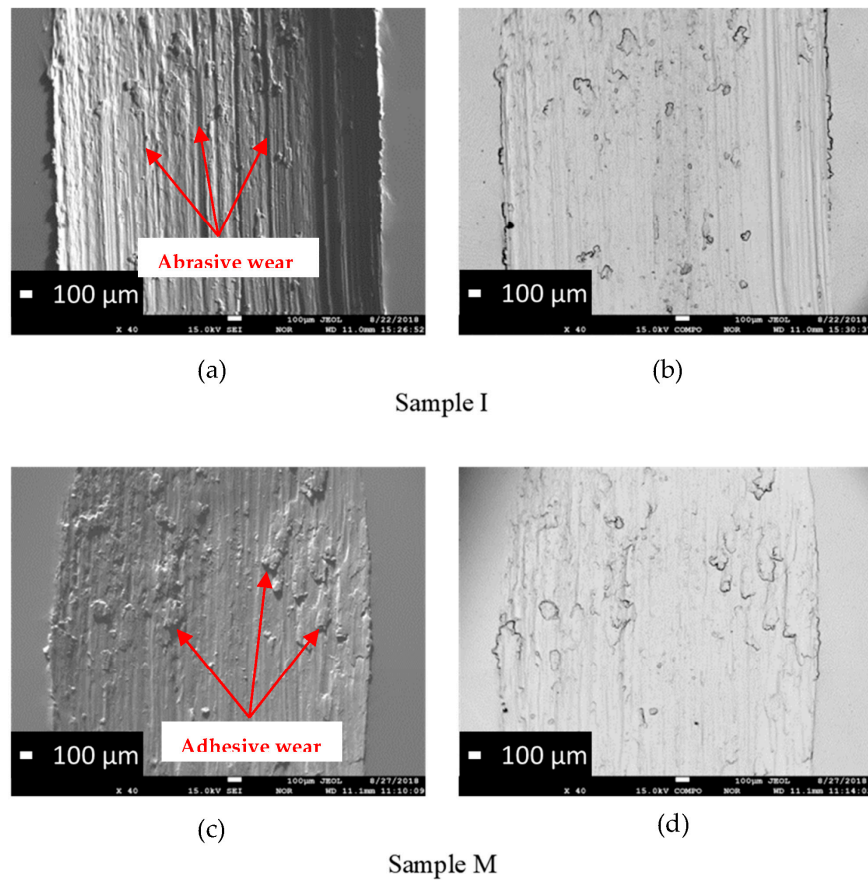


Figure 11. SEM images of the wear tracks. (a) Secondary electron imaging for Sample I; (b) back-scattered electron imaging for Sample I; (c) Secondary electron imaging for Sample M; (d) back-scattered electron imaging for Sample M.

A more detailed analysis of back-scattered electron images with semiquantitative element composition analysis via EDS reveals that the sliding action promoted the formation of a tribolayer with the presence of oxygen in Sample I, as indicated in Figure 12. However, as observed in Figure 13, in Sample M, such an analysis did not identify the presence of oxygen. From the literature [25], oxidation phenomena occur due to wear heat and an oxidized layer, which protects the surface against subsequent wear damage. This phenomenon may help explain the higher wear resistance observed in Sample I and agrees with the results found by Chen et al. [26] when using a thermal spraying process to produce Inconel 625 coatings.

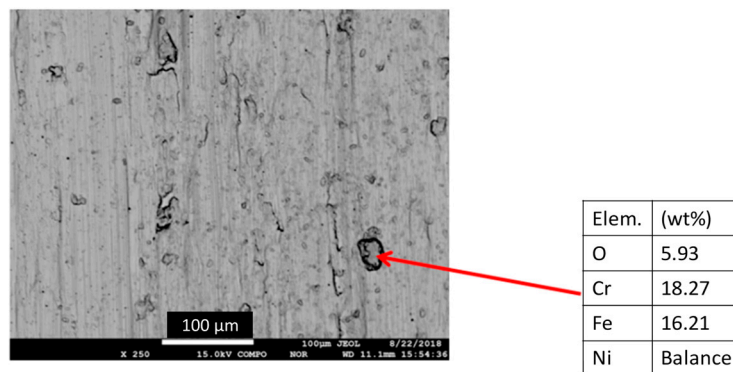


Figure 12. Back-scattered electron image details and semiquantitative element composition (EDS) of Sample I (Inconel 625 weld layer).

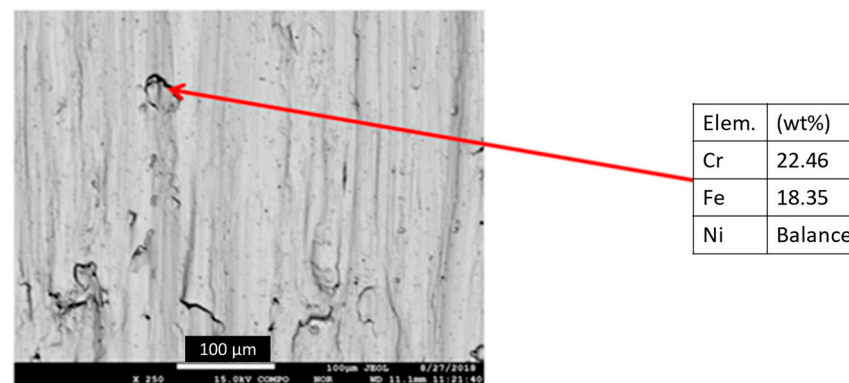


Figure 13. Back-scattered electron image details and semiquantitative element composition (EDS) of Sample M (stainless-steel 316LSi intermediate weld layer followed by the top Inconel 625 weld layer).

Based on the results gathered throughout this study, it is reasonable to suppose that the addition of the Inconel overlay produced via GMAW cladding directly on top of carbon steel reduces the wear rate, while the addition of Inconel on top of an intermediate stainless-steel layer increases the wear rate despite keeping a friction coefficient compared to that obtained when coating using Inconel only.

4. Conclusions

The present work aimed to compare the tribological behavior under the sliding wear of the Inconel 625 overlay produced on top of carbon and stainless steels via the GMAW cladding process. According to the analysis tools that were employed and based on their results, the following conclusions can be drawn:

- The analysis of the cladding layers revealed a columnar dendritic structure with respect to the Inconel on top of carbon steel used as a substrate and a cellular structure with respect to the Inconel on top of stainless steel used as a substrate.
- An increase in the amount of Nb was observed in the layer deposited over 316LSi. This increase likely led to an increase in the number of precipitates and/or Laves phase formation.
- The sliding wear tests revealed similar friction coefficients for both cladding sequences (with and without the intermediate layer).
- Although there were no significant differences in chemical composition, hardness, and friction coefficient, the Inconel weld layer showed greater resistance to wear probably due to the difference in the morphology of the microstructure that formed.
- The samples revealed different predominant wear mechanisms; abrasive wear in the Inconel weld layer and adhesive wear in the stainless-steel intermediate weld layer followed by the top Inconel weld layer.

Author Contributions: Conceptualization and methodology, D.S., D.F.F. and J.L.G.J.; welding coats fabrication, A.F.T.; microstructural characterization, D.S., D.F.F. and J.L.G.J.; hardness characterization, D.F.F.; sliding wear, J.L.G.J. and W.M.D.S.J.; formal analysis, D.S., D.F.F., J.L.G.J. and R.P.R.; writing—original draft preparation, D.S., D.F.F., J.L.G.J. and R.P.R.; writing—review and editing, R.P.R.; funding acquisition, D.F.F. All authors have read and agreed to the published version of the manuscript.

Funding: This research was funded by Brazilian National Council for Scientific and Technological Development (CNPq), grant numbers 457637/2014-5 and 305636/2021-9, FAPEG, FAPEMIG, and CAPES.

Institutional Review Board Statement: Not applicable.

Informed Consent Statement: Not applicable.

Data Availability Statement: No new data were created or analyzed in this study. Data sharing is not applicable to this article.

Acknowledgments: The authors acknowledge the financial support from the Brazilian National Council for Scientific and Technological Development (CNPq), via grants 457637/2014-5, and 305636/2021-9, FAPEG, FAPEMIG, CAPES and the infrastructural support from LAMAF/EMC/UFG, CRTi/UFG, and LTM/UFU.

Conflicts of Interest: The authors declare no conflict of interest.

References

1. Abioye, T.E.; McCartney, D.G.; Clare, A.T. Laser cladding of Inconel 625 wire for corrosion protection. *J. Mater. Process. Technol.* **2015**, *217*, 232–240. [CrossRef]
2. Soares, J.P.; Terrones, L.A.H.; Paranhos, R. Efeito dos Tratamentos Térmicos de Normalização e de Solubilização na Microestrutura de uma Junta Dissimilar Soldada entre um Tubo de Aço API 5L X-52 e o Inconel 625. *Soldag. Inspeção* **2017**, *22*, 357–373. [CrossRef]
3. Sandes, S.S.; Alvarães, C.P.; Mendes, M.C.; Araújo, L.S.; de Souza, L.F.G.; Jorge, J.C.F. Avaliação de Revestimentos de Liga de Níquel 625 Depositados pelo Processo Eletroescória. *Soldag. Inspeção* **2016**, *21*, 417–427. [CrossRef]
4. Fesharaki, M.N.; Shoja-Razavi, R.; Mansouri, H.A.; Jamali, H. Microstructure investigation of Inconel 625 coating obtained by laser cladding and TIG cladding methods. *Surf. Coat. Technol.* **2018**, *353*, 25–31. [CrossRef]
5. Antoszczyszyn, T.J.; Paes, R.M.G.; de Oliveira, A.S.C.M.; Scheid, A. Impact of dilution on the microstructure and properties of Ni-based 625 alloy coatings. *Soldag. Inspeção* **2014**, *19*, 134–144. [CrossRef]
6. Zhang, Y.; Pan, Q.; Yang, L.; Li, R.; Dai, J. Tribological Behavior of IN718 Superalloy Coating Fabricated by Laser Additive Manufacturing. *Lasers Manuf. Mater. Process.* **2017**, *4*, 153–167. [CrossRef]
7. Khadem, M.; Penkov, O.V.; Yang, H.-K.; Kim, D.-E. Tribology of multilayer coatings for wear reduction: A review. *Friction* **2017**, *5*, 248–262. [CrossRef]
8. Wang, H.; Ma, G.; Xu, B.; Yong, Q.; He, P. Design and application of friction pair surface modification coating for remanufacturing. *Friction* **2017**, *5*, 351–360. [CrossRef]
9. Cai, Z.; Chen, Z.; Sun, Y.; Jin, J.; Peng, J.; Zhu, M. Development of a novel cycling impact-sliding wear rig to investigate the complex friction motion. *Friction* **2019**, *7*, 32–43. [CrossRef]
10. Li, J.; Lu, Y.; Zhang, H.; Xin, L. Effect of grain size and hardness on fretting wear behavior of Inconel 600 alloys. *Tribol. Int.* **2015**, *81*, 215–222. [CrossRef]
11. ASTM A36; Standard Specification for Carbon Structural Steel. ASTM International: West Conshohocken, PA, USA, 2019.
12. Weld Inox. WI N 316LSi. Diadema, São Paulo. Available online: <https://www.weldinox.com.br/produto-informacoes?id=352> (accessed on 1 March 2022).
13. Weld Inox. WI N 6250. Diadema, São Paulo. Available online: <https://www.weldinox.com.br/produto-informacoes?id=419#produtoInt-sup> (accessed on 1 March 2022).
14. dos Santos, M.B.; Costa, H.L.; De Mello, J.D.B. Potentiality of triboscopy to monitor friction and wear. *Wear* **2015**, *332–333*, 1134–1144. [CrossRef]
15. Belin, M. Triboscopy: A new quantitative tool for microtribology. *Wear* **1993**, *168*, 7–12. [CrossRef]
16. Belin, M.; Lopez, J.; Martin, J.M. Triboscopy, a quantitative tool for the study of the wear of a coated material. *Surf. Coat. Technol.* **1994**, *70*, 27–31. [CrossRef]
17. Bozzi, A.C.; de Mello, J.D.B. Triboscopia: Princípios potencialidades da técnica e aplicação em ensaios de desgaste por deslizamento. In Proceedings of the 61^o Congresso Anual da ABM, Rio de Janeiro, Brazil, 24–27 July 2006; pp. 4010–4018.
18. Kim, J.S.; Park, Y.I.; Lee, H.W. Effects of heat input on the pitting resistance of Inconel 625 welds by overlay welding. *Met. Mater. Int.* **2015**, *21*, 350–355. [CrossRef]
19. Souza, D.; Vilhalba, L.B.; Passos, T.A.; Moura, E.A.M.; Costa, H.L.; Osorio, A.G. Corrosion resistance of thermal-pulsed Inconel 625 MIG/MAG weld overlays. *Surf. Topogr. Metrol. Prop.* **2021**, *9*, 025036. [CrossRef]
20. Lin, C. Relationships between microstructures and properties of buffer layer with Inconel 52M clad on AISI 316L stainless steel by GTAW processing. *Surf. Coat. Technol.* **2013**, *228*, 234–241. [CrossRef]
21. Bergman, T.L.; Lavine, A.S.; Incropera, F.P.; Dewitt, D.P. *Fundamentals of Heat and Mass Transfer*; John Wiley & Sons, Inc.: Hoboken, NJ, USA, 2011.
22. Sun, R.; Qiao, Y.; Li, X.; Shi, Y.; Wang, X. Microstructure, Wear Resistance and Corrosion Performance of Inconel 625 Layer Fabricated by Laser/Ultra-High Frequency (UHF) Induction Hybrid Deposition. *Processes* **2023**, *11*, 1118. [CrossRef]
23. Najafi, M.; Moshkbar Bakhshayesh, M.; Farzadi, A. Microstructure and Phase Analysis of Multilayer Ni–Cr–Mo Clad for Corrosion Protection. *Trans. Indian Inst. Met.* **2021**, *74*, 1663–1672. [CrossRef]
24. Sauraw, A.; Sharma, A.K.; Fydrych, D.; Sirohi, S.; Gupta, A.; Świerczyńska, A.; Pandey, C.; Rogalski, G. Study on Microstructural Characterization, Mechanical Properties and Residual Stress of GTAW Dissimilar Joints of P91 and P22 Steels. *Materials* **2021**, *14*, 6591. [CrossRef]

25. Evangeline, A.; Sathiya, P. Cold metal arc transfer (CMT) metal deposition of Inconel 625 superalloy on 316L austenitic stainless steel: Microstructural evaluation, corrosion and wear resistance properties. *Mater. Res. Express* **2019**, *6*, 066516. [[CrossRef](#)]
26. Chen, T.; Chou, C.; Yung, T.; Cai, R.; Huang, J.; Yang, Y. A comparative study on the tribological behaviour of various thermally sprayed Inconel 625 coatings in a saline solution and deionized water. *Surf. Coat. Technol.* **2020**, *385*, 125442. [[CrossRef](#)]

Disclaimer/Publisher's Note: The statements, opinions and data contained in all publications are solely those of the individual author(s) and contributor(s) and not of MDPI and/or the editor(s). MDPI and/or the editor(s) disclaim responsibility for any injury to people or property resulting from any ideas, methods, instructions or products referred to in the content.